Physica Medica 52 (2018) 113–121

Contents lists available at ScienceDirect

Physica Medica

journal homepage: www.elsevier.com/locate/ejmp

Original paper

Miniaturized microdosimeters as LET monitors: First comparison of calculated and experimental data performed at the 62 MeV/u ^{12}C beam of INFN-LNS with four different detectors

P. Colautti[a,*], V. Conte[a], A. Selva[a], S. Chiriotti[b], A. Pola[c,d], D. Bortot[c,d], A. Fazzi[c,d], S. Agosteo[c,d], M. Treccani[c,d], L. De Nardo[e,f], C. Verona[g,h], G. Verona Rinati[g,h], G. Magrin[i], G.A.P. Cirrone[j,k], F. Romano[j,l]

[a] INFN Laboratori Nazionali di Legnaro, viale dell'Università 2, 35020 Legnaro, Italy
[b] Belgian Nuclear Research Centre, SCK·CEN, Boeretang 200, 2400 Mol, Belgium
[c] Politecnico di Milano, Dipartimento di Energia, via La Masa 34, 20156 Milano, Italy
[d] INFN, Sezione di Milano, via Celoria 16, 20133 Milano, Italy
[e] INFN, Sezione di Padova, via Marzolo 8, 35131 Padova, Italy
[f] University of Padova, Physics and Astronomy Department, via Marzolo 8, 35131 Padova, Italy
[g] INFN, Sezione di Roma Tor Vergata, via della Ricerca Scientifica, 1, 00133 Roma, Italy
[h] University of Roma Tor Vergata, via del Politecnico 1, Roma 00133, Italy
[i] EBG MedAustron, Marie Curie-St. 5, 2700 Wiener Neustadt, Austria
[j] INFN Laboratori Nazionali del Sud, via S.Sofia 62, 95123 Catania, Italy
[k] ELI-Beamlines, Za Radnici 835, Dolní Břežany 252 41, Czech Republic
[l] ELI-National Physical Laboratory, CMES – Medical Radiation Science, Teddington, UK

ABSTRACT

Purpose: The aim of this paper is to investigate the limits of LET monitoring of therapeutic carbon ion beams with miniaturized microdosimetric detectors.

Methods: Four different miniaturized microdosimeters have been used at the 62 MeV/u ^{12}C beam of INFN Southern National Laboratory (LNS) of Catania for this purpose, i.e. a mini-TEPC and a GEM-microdosimeter, both filled with propane gas, and a silicon and a diamond microdosimeter. The $\bar{y}_D$ (dose-mean lineal energy) values, measured at different depths in a PMMA phantom, have been compared with $L\bar{E}T_D$ (dose-mean LET) values in water, calculated at the same water-equivalent depth with a Monte Carlo simulation setup based on the GEANT4 toolkit.

Results: In these first measurements, no detector was found to be significantly better than the others as a LET monitor. The $\bar{y}_D$ relative standard deviation has been assessed to be 13% for all the detectors. On average, the ratio between $\bar{y}_D$ and $L\bar{E}T_D$ values is 0.9 ± 0.3, spanning from 0.73 ± 0.08 (in the proximal edge and Bragg peak region) to 1.1 ± 0.3 at the distal edge.

Conclusions: All the four microdosimeters are able to monitor the dose-mean LET with the 11% precision up to the distal edge. In the distal edge region, the ratio of $\bar{y}_D$ to $L\bar{E}T_D$ changes. Such variability is possibly due to a dependence of the detector response on depth, since the particle mean-path length inside the detectors can vary, especially in the distal edge region.

1. Introduction

Ion beam therapy is a technique that uses fast light ions (mainly protons and carbon ions) to treat radio-resistant tumours. The use of this technique is steadily increasing worldwide because of its favourable depth-dose distribution and lesser lateral spread with respect to the traditional radiation fields used in radiotherapy (photons and electrons). Differently from photon, electron or neutron beams, the energy loss of ions is highest at the end of the penetration range, giving rise to the so-called Bragg-peak. This favourable physical property of ion beams is exploited in therapy to provide excellent dose conformity to the volume of solid state tumours, sparing healthy tissues and avoiding organs at risk better than conventional radiotherapy. At present, there are seventy-three therapeutic centres treating patients with particle beams [1]. Most of them use fast proton beams, whereas eleven centres (4 in Europe, 5 in Japan and 2 in China) employ carbon ion beams. Carbon ions offer, beside the favourable physical properties, also biological advantages over protons: higher relative-biological-effectiveness

* Corresponding author.
E-mail address: paolo.colautti@lnl.infn.it (P. Colautti).

https://doi.org/10.1016/j.ejmp.2018.07.004
Received 8 March 2018; Received in revised form 10 July 2018; Accepted 11 July 2018
Available online 18 July 2018

(RBE) and lower oxygen-enhancement-ratio (OER) [2,3]. The RBE enhancement and the OER lowering are related to the increasing of the electronic stopping power (here called linear-energy transfer or simply LET), as pointed out by several radiobiological studies performed at different LET values [4]. These features make carbon ions more suitable to treat tumours that are resistant to relatively low-LET radiation fields.

The LET value of a mono-energetic ion beam penetrating into tissue can be easily calculated. However, as a result of the nuclear collisions, the interactions of high-energy carbon ions with tissue give rise to a complex mixed radiation field [5], which is populated by different particles with different LET values. Besides, the relative components of such particle population change both with depth and with lateral distance from the pristine ion trajectory. In mixed radiation fields, a valuable parameter to assess RBE and OER mean values could be the averaged dose-mean LET value ($L\bar{E}T_D$) [6]. It can be calculated with a Monte Carlo (MC) model capable of transporting all the primary and secondary particles. The limitations of MC codes are the uncertainties on the cross sections, the accuracy of the physical models and the calculation time. An experimental monitoring of the $L\bar{E}T_D$ of the therapeutic beam could be a fast way to improve RBE and OER assessment in the real treated volume. However, even if microdosimeters are not LET detectors, they can perform in-beam measurements with a good precision. Microdosimeters are gas or solid-state detectors, which measure the spectrum of ionization events occurring in a given site, namely inside their sensitive volumes, at the passage of a single ionizing particle (see Section 2). The measured quantity is the lineal energy y, which, differently from LET, is a stochastic quantity. However, the mean weighted value of a microdosimetric spectrum (called dose-mean lineal energy or $\bar{y}_D$ [7]) is, in first approximation, proportional to $L\bar{E}T_D$. Therefore, $\bar{y}_D$ could be used to monitor the $L\bar{E}T_D$of a carbon ion therapeutic beam; hence as a basis for the estimation of RBE and OER values.

At present, four detectors have the technical features to perform microdosimetric measurements in carbon ion beams used in hadrontherapy centres: the mini-TEPC [8], the GEM microdosimeter [9], the silicon microdosimeter [10] and the diamond microdosimeter [11]. Since they are different in shape and constructive materials, their spectra are not expected to be equal, but the $\bar{y}_D$ values could be less sensitive to the spectral differences, since they are average values. Furthermore, such differences, although significant for LET monitoring, could be not so relevant for RBE and OER assessment, given the uncertainty in the correlation between LET and radiobiological data.

This study compares the $\bar{y}_D$ values measured by these four detectors in a PMMA phantom with $L\bar{E}T_D$values calculated in water by means of GEANT4 code [12]. The 62 MeV/u ^{12}C beam of INFN Laboratories of Catania has been used. The aim of this research is twofold: the first aim is to study how much the constructive differences of the four detectors change the measured $\bar{y}_D$ value, while the second is to study the limits of $\bar{y}_D$ as a $L\bar{E}T_D$ monitor (in liquid water) by investigating the variation with depth of the proportionality factor between these two quantities. Although the quantity used in radiation therapy to assess RBE and OER is the $L\bar{E}T_D$ in water, these first measurements have been performed in a PMMA phantom, scaling the PMMA depth to the water-equivalent one.

2. Microdosimeter limits as $L\bar{E}T_D$ detectors

LET is the mean energy loss per unit path length of a charged particle of given energy in a given material and it is defined for mono-energetic beams [13]. In a site of finite size, the LET value changes due to the degradation of the incident particle. There are two common definitions of mean LET in a finite volume: the track averaged LET (L_T), where the average is carried out on equal path length, and the dose averaged LET (L_D), where it is carried out on equal contributions to the absorbed dose. In any case, LET is not defined for a mixed radiation field. Therefore, in this paper we have followed the definition of F. Romano et al. [6] for therapeutic ion beams, which defines the dose mean LET at a given depth in a phantom, $L\bar{E}T_D$. According to this definition, $L\bar{E}T_D$ is the average of the dose-mean LET values of all charged particles at a given depth, weighted with the relative contribution of each particle to the absorbed dose.

The microdosimetric spectrum is the spectrum of the size of ionisation events due to a single particle in the detector sensitive volume, the thickness of which is expressed, in this paper, in mg/cm^2 or in micrometres of water-equivalent thickness.

If we assume that the energy needed to create an ion pair in the microdosimeter is, with good approximation, the same for all interacting charged particles, the ionisation pulse-height spectrum originated by a single particle can be calibrated in imparted-energy per single event ε_s by using an alpha source of known energy or a noticeable physical point in the microdosimetric spectrum (electron edge, proton edge, carbon ion edge). The microdosimetric spectrum can then be read as the probability of occurrence of a "lineal energy" event of size y, defined as the ratio $\frac{\varepsilon_s}{\bar{l}}$, where $\bar{l}$ is the sensitive-volume mean chord-length [14]. For fundamental physical reasons, the y-value fluctuates also if it is due to a mono-energetic particle of a precise LET value. Therefore, the lineal energy is a stochastic variable, differently from LET, which is an average value. This means that only microdosimetric mean values can approximate LET values of a mixed radiation field. In fact, if we assume that the energy loss straggling of charged particles, the secondary electron (δ-ray) escape and the LET variation inside the sensitive volume can be neglected (continuous slowing-down approximation, CSDA), the mean energy imparted $\bar{\epsilon}$ in the site by an ionising particle is the product of the particle LET and its path length in the detector sensitive volume. These assumptions are reasonable for particles with a range greater than the detector sensitive volume and for which the δ-ray penumbra around the track is smaller than the sensitive volume itself. In these conditions, $\bar{y}_D$is proportional to $L\bar{E}T_D$. The proportionality factor depends on the mean path-length distribution in the sensitive volume, which in turns depends on the sensitive volume shape when particles cross randomly the volume [15]. However, when the radiation field is anisotropic, $\bar{y}_D$ depends also on the detector orientation with respect to the field, unless the sensitive volume is spherical and the beam is uniform over the sensitive volume cross section. Unfortunately, it is not easy to construct miniaturized spherical microdosimeters able to accurately measure in therapeutic ion beams, since the sensitive volume size has to be 1 mm or less (see later on). Since the sensitive volumes of the four detectors considered in this work are not spherical, the proportionality factors between $\bar{y}_D$ and $L\bar{E}T_D$ are unknown, because they depend also on the radiation field anisotropy, which changes with depth inside the phantom due to beam straggling and secondary particle production. If the radiation field anisotropy can be assumed to be approximately constant, the following equation is valid at any depth:

$$\overline{LET_D} = k \cdot \bar{y}_D \tag{1}$$

being the proportional factor k different for each detector. In such a case the goodness of a microdosimeter as $L\bar{E}T_D$ monitor can be reduced to the invariance of k with depth.

Another limit of microdosimeters as LET monitors is the maximum sustainable rate of ions impinging on the detector. With the active scanning modality in a therapeutic ^{12}C beam, microdosimeters have to stand fluence rates of at least $10^7 \cdot cm^{-2} s^{-1}$. That means they must have geometrical cross section of ~1 mm^2 or less [16] to prevent pulse pile-up and microdosimetric spectral distortions, giving rise to wrong $\bar{y}_D$ measurements. Since it is complicated to manufacture millimetric spherical counters, miniaturized microdosimeters are usually small cylinders, whose response depends on their orientation with respect to the radiation field. However, since the therapeutic carbon ion field cannot be assumed isotropic, the detector mean chord length $\bar{l}$ cannot be precisely calculated without knowing the space and vector-velocity

distributions of impinging particles. Therefore, the accuracy of a microdosimeter as LET monitor is matter for experimental verification.

3. Calibration of microdosimeters

The microdosimetric spectrum is generally obtained by joining two or three sub-spectra measured with different pulse amplifications. In order to perform a precise junction, these sub-spectra are first calibrated in volt or charge per pulse, after a careful check of the electron chain linearity. In this work, the calibration in terms of lineal energy y was performed by considering the carbon edge as a distinctive region of the microdosimetric spectrum formed by events of known imparted energy. The same procedure was already adopted with the proton edge [17,18] and with the electron edge [19], see Section 2.

The carbon edge is the spectral region where the number of pulses per acquisition channel drops sharply, corresponding to the maximum amount of energy imparted by carbon ions to the sensitive volume. The initial height of this region is greater when the relative number of carbon ions with stopping power close to the maximum value is higher. That happens at depths close to the 62 MeV/u carbon ion range. In our measurements, this spectral region is easily recognisable in the pulse height spectrum collected at the water-equivalent depth of 7.9 mm. Since the sensitive volume thickness of the four microdosimeters is smaller than the range of ions having the maximum LET, and the LET variation in the volume itself can be neglected, a correspondence between the pulse height at the edge and the maximum stopping power of carbon ions in the sensitive volume material can be made. To better define the carbon edge value, the region where the number of pulses drops abruptly has been best fitted with the Fermi-like function:

$$h \cdot d(h) = \frac{A}{1 + e^{B \cdot (h - c)}} \tag{2}$$

where h is the pulse height (in volts), $d(h)$ is the dose distribution of h and A, B, C are fitting parameters. The Fermi function is a monotonically decreasing function. The intercept of the tangent at the inflection point with the abscissa axis has been chosen as the most precise marker point of the edge. This value, called h_{edge}, is:

$$h_{edge} = 2/B + C \tag{3}$$

(see reference [19] for more details). For all the detectors, the calibration was eventually performed by assigning to this marker the value of the maximum stopping power of carbon ions in liquid water (LET_{max}), which is 976 keV/μm. This calibration procedure, which is independent of the sensitive volume material, assumes that the scaling factor to convert the measured pulse-height values h [volt] to the y values in water [keV/μm] is the same for any lineal energy, and that the dependence on the sensitive volume material is included in the factor k of equation (1).

4. The microdosimeters

4.1. The propane-based mini-tepc

The mini-TEPC has a cylindrical sensitive volume 0.9 mm in diameter and height, surrounded by a 0.35 mm-thick A-150-cathode wall, a 0.35 mm Rexolite® insulator, and a 0.2 mm-thick aluminium sleeve for a total external diameter of 2.7 mm. The detector is inserted inside a 160-mm-long aluminium sleeve. The mini-TEPC operates in gas-flow modality. The detector is connected with the gas line and the vacuum line through Swagelok® quick connectors. A picture of the detector is shown in Fig. 1. The mini-TEPC is filled with propane gas. The gas pressure inside the counter is maintained constant with Baratron® absolute manometers, a mass-flow controller, an electromagnetic solenoid valve and a control system (MKS Instruments). Individual pulses from the preamplifier are fed into a NIM/CAMAC/PC based data acquisition system for analogue and digital signal processing. More details are given in reference [8].

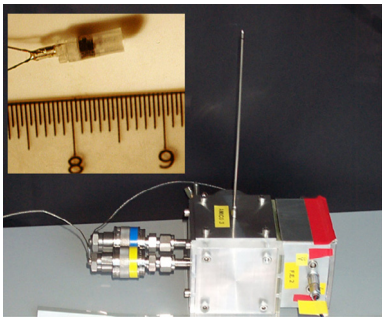

Fig. 1. The mini-TEPC (black cylinder inside the Rexolite® cylinder in the inset) and the detector holder (the long stick), which is in turn inserted in the aluminium box that contains the front-end electronics and the vacuum and gas ports.

4.1.1. Mini-TEPC experimental setup and data processing

The detector was placed up-side down in a PMMA phantom (as shown in Fig. 5). The sensitive volume was aligned with the centre of the ^{12}C beam, the diameter of which was 25 mm. The depth in the phantom was determined by placing a stack of PMMA layers of different thickness between the counter and the beam collimator. The PMMA-equivalent wall thickness of the detector is 1.16 mm. It has been calculated using the average mass stopping-power ratio of carbon ions in the different materials composing the detector wall. This value has been added to the PMMA layer thickness to obtain the total depth. A PMMA beam stopper was placed downstream of the detector.

All the measurements were performed at low gas gain with the anode wire grounded through the pre-amplifier and the cathode wall biased at −600 V. Three spectroscopy linear amplifiers of different gains were used to shape and amplify simultaneously pulses from the preamplifier. In order to minimize pulse pile-up, the amplifier shaping times were set to 250 ns (the minimum value allowed by the electronics). The three sub-spectra were calibrated in volt with a research pulse generator and then joined to obtain the microdosimetric spectrum. All the measurements were performed in gas-flow modality (1 $cm^3 \cdot min^{-1}$) at a pressure of 45.4 kPa of propane at a temperature of 21.8 °C; in these conditions the sensitive volume mass thickness is 0.075 mg/cm^2, which is equivalent, in terms of mean imparted energy, to 0.83 μm of liquid water ($0.075 \cdot (\bar{S}_\rho)_{propane} / (S_\rho)_{water}$, where the stopping power ratio is averaged over all the carbon ion energy range).

The spectrum energy calibration was performed by using the carbon edge technique (see Section 3). The carbon edge is well defined at 6.5 mm of PMMA total depth (equivalent to 7.9 mm of water-equivalent depth, see Section 7.1). At the carbon edge, the carbon ion range in propane (0.46 mg/cm^2) is larger than the sensitive volume thickness (0.075 mg/cm^2). Therefore, the spectrum collected at this depth was calibrated following the procedure described in Section 3. Namely, the value of 976 keV·μm^{-1} (corresponding to the maximum LET value of carbon ions in liquid water [20]) was assigned to the intercept with the abscissa axis of the tangent at the inflection point of the fitting function. The calibration factor applied to the spectrum at 7.9 mm of water-equivalent depth was used to calibrate also the spectra collected at different depths.

The lower detection threshold was ~2 keV/μm. To take into account also energy deposition events below this threshold, the frequency spectra $f(y)$ were first linearly extrapolated down to 0.01 keV/μm and then processed to obtain the $yd(y)$ against the ln(y) distribution and the $\bar{y}_D$ value.

All the measurements were performed at counting rates lower than $2 \cdot 10^4\ s^{-1}$.

4.2. The propane-based gem microdosimeter

The GEM microdosimeter is a matrix of 16 independent mini-TEPC-like counters uniformly distributed over a 144 mm^2 area. The detector was conceived to measure the microdosimetric beam quality and its uniformity in space with a single data acquisition. The main elements of the detector are a cathode, made of A-150 plastic 1 mm in thickness, a GEM foil, with a sensitive area of 5 × 5 cm^2, and a readout printed circuit board (PCB), with 16 circular pads 2 mm in diameter, disposed in a 4 × 4 matrix (pitch of 4 mm). The GEM structure used in this work is the so-called standard GEM, that is a Kapton foil 50 μm in thickness with a 5 μm-thick copper coating on each side, perforated on a triangular pattern (pitch of 140 μm) with holes having a double conical shape (the diameters in the copper surfaces and in the Kapton are 70 and 50 μm, respectively). A single charged particle gives rise to ionisations in the drift region (the space between the cathode and the GEM). The electrons drift towards the GEM, where they are multiplied. The electronic avalanche is collected by circular anodes 2 mm in diameter that are placed 0.5 mm behind the GEM (the so-called induction gap). The drift region gap and the anode diameters define 16 almost wall-less sensitive volumes, which are cylinders 2 mm in height and diameter (see Fig. 2). The detector is inserted in a vacuum tight chamber (21.5 × 14.8 × 8.0 cm^3) equipped with gas-in and gas-out ports, instrumentation for gas pressure control in flow modality and electrical connectors. The beam enters into the chamber through a flange with a Kapton window 25 μm in thickness and 28 mm in diameter. Eventually, the beam impinges on the GEM detector parallelly to the sensitive volume axes (from the top in Fig. 2). The detector operates in gas flow modality by using a Baratron® absolute manometer, a mass-flow controller, an electromagnetic solenoid valve and a control system (MKS Instruments). Propane gas was used. More details are given in reference [9].

4.2.1. GEM-microdosimeter experimental setup and data processing

The detector was placed in the PMMA phantom. The depth in the phantom was determined by placing a stack of PMMA layers of different thickness between the counter window and the beam collimator, the diameter of which was 25 mm. The PMMA-equivalent detector-wall thickness has been calculated to be 0.99 mm. This thickness has been added to that of the PMMA layers to obtain the total depth in the phantom.

In these measurements, the signals induced in only four out of sixteen mini-TEPC-like counters were acquired at the same time to check the uniformity of the microdosimetric quality of the beam. Charges collected on four readout pads were fed into charge preamplifiers and pulses were then directly sent to a CAEN DT5724 Digitizer (4 Channel 14 bit 100 MS/s) equipped with DPP-PHA Firmware (Digital Pulse Processing for the Pulse Height Analysis) controlled by a PC. This provides a digital pulse spectrum equivalent to that from a shaping amplifier plus a peak sensing ADC. All the measurements were performed with the anode pads grounded through the preamplifiers, a voltage difference between the two sides of the GEM ΔV_{GEM} = 330 V, a drift field E_D = 0.45 kV/cm and an induction field E_I = 3.0 kV/cm. All the measurements were performed in gas-flow modality (1 $cm^3 \cdot min^{-1}$) at a pressure of 21 kPa of propane and at a temperature of 21.8 °C; at this pressure the sensitive volume mass thickness is 0.077 mg/cm^2, equivalent, in terms of mean imparted energy, to 0.86 μm in liquid water.

The spectra were calibrated by using the carbon edge of the spectrum at 6.5 mm of PMMA depth (7.9 mm of water-equivalent depth), similarly to what was done for the mini TEPC (see Section 4.1.1), since the sensitive volume thickness is smaller than the range in propane of carbon ions with maximum LET (0.46 mg/cm^2). The lower detection threshold was ~2 keV/μm. Therefore, *f(y)* spectra were first extrapolated linearly down to 0.01 keV/μm, in order include the contribution of the ionization events below the detection threshold, and then processed to obtain the *yd(y)* against ln(*y*) distribution and the $\bar{y}_D$ value.

At all depths the spectra of the four mini-TEPC-like counters were processed in the same way. No significant difference was observed among them both in $\bar{y}_D$ values and *yd(y)* distributions. This finding confirms the uniformity of the carbon ion beam at least over the 144 mm^2 area at the centre. Therefore, the response of only one mini-TEPC-like counter was used for the comparison, reducing the GEM counter sensitive volume to a cylinder of 2 mm in diameter and height (equivalent to a cylinder of 0.86 μm of water in diameter and height).

4.3. The silicon microdosimeter

The silicon microdosimeter is a two-stage detector consisting of a single thin Δ*E* stage (about 1.9 μm in thickness and 1 mm^2 in sensitive area) coupled with a thick *E* stage (about 700 μm in thickness), as shown in Fig. 3. The silicon thickness of 1.9 μm (density 2.3 $g \cdot cm^{-3}$) is equivalent, in terms of mean imparted energy, to 3.3 μm of water, since the mean ratio of mass stopping-power of silicon to water is 0.75 [20]. Both the ΔE and the E stages are biased and the respective signals are amplified and shaped by using two independent electronic chains. The electronic signals generated in the two stages are acquired by a two-channel ADC in coincidence mode. In this detector, the ΔE-stage signals give rise to the microdosimetric spectrum, while the E-stage signals allow for particle discrimination, and therefore to separate the spectral components due to different charged particles.

4.3.1. Silicon-microdosimeter experimental set-up and data processing

The silicon telescope was assembled to be shielded from electromagnetic interferences and was placed in the PMMA phantom (as shown Fig. 3). The experimental set-up was the same as for the mini-TEPC microdosimeter. The silicon sensitive volume was aligned with the centre of the ^{12}C beam (25 mm in diameter) and the depth in the phantom was determined by placing a stack of PMMA layers of different thickness between the telescope and the beam collimator. The detector wall thickness was 0.0 mm.

In these measurements, only the ΔE signals were acquired, since the E-stage signals could not be used for particle discrimination. In fact, the E-stage is too thin with respect to the range in silicon of the ions with

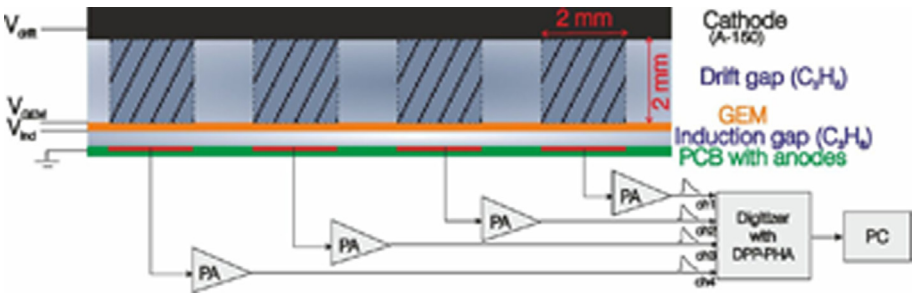

Fig. 2. Draft of the GEM microdosimeter. The dark grey squares are a cross-sectional view of four cylindrical sensitive volumes, the signals of which are collected in parallel. The ion beam enters into the detector from the top of the figure, parallel to the sensitive volume axis.

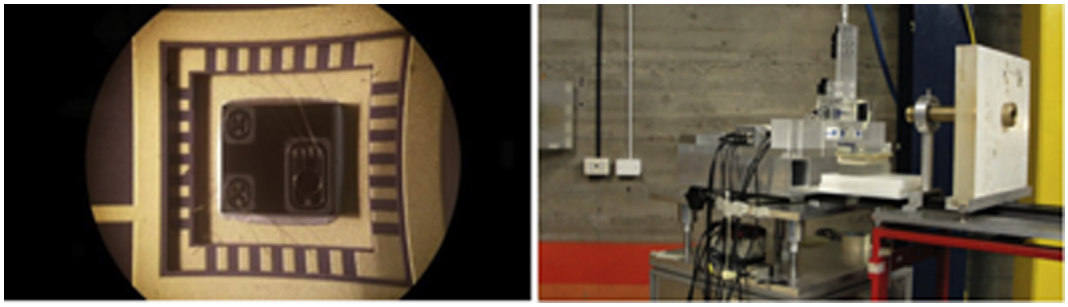

Fig. 3. The silicon telescope is the black 1 mm circle inserted in the right side of the black square of the electronic chip (left side of the figure). On the right side, the fully assembled detector on the carbon ion beam line is shown.

the highest energies and therefore their initial energy cannot be assessed. Measured pulses were first calibrated by injecting known amounts of charge through the preamplifier test input (capacitance 4.7 pF). The carbon edge in silicon is due to ions which have a range of 0.97 mg/cm^2, larger than the sensitive volume thickness (0.437 mg/cm^2). Therefore, the spectra were calibrated following the procedure described in § 3. The lower detection threshold was ~10 keV/μm. Eventually, *f(y)* spectra were extrapolated linearly down to 0.01 keV/μm and then processed to obtain the *yd(y)* against ln(*y*) distribution and the $\bar{y}_D$ values.

4.4. The diamond microdosimeter

The diamond-based microdosimeter is a multi-layer structure obtained by a two-step growing procedure through the Microwave Plasma Enhanced CVD (MWPECVD) technique, by using two different growing apparata. The fabrication process of the detectors is described in detail in reference [21]. The detector sensitive volume is a small square (0.3 × 0.3 mm^2) of intrinsic high purity and high quality CVD diamond. The thickness of the sensitive volume is 2.0 μm (density 3.5 g·cm^{-3}), which is equivalent, in terms of mean imparted energy, to 6.1 μm of water (the average mass stopping-power ratio diamond/water is 0.87 [20]). The diamond-based microdosimeter is schematically shown in the left side of Fig. 4. This detector operates in sandwich geometry in order to exploit the internal junction electric field. The detector is in practice a p-i-metal structure with the metallic rectifying contact having a Schottky barrier of about 1.2 eV, as deduced from previous experimental studies [22]. For this reason, the particular detector structure used is able to operate without any external applied voltage, as a result of its internal junction electric field. All measurements reported in this work were performed with no external bias voltage applied. The back contact (boron doped diamond layer) was grounded, while the top contact (Cr layer) was connected to a conventional charge-sensitive electronic chain, consisting of a charge-sensitive preamplifier Amptek A250CF – CoolFET and an Ortec 671 shaping amplifier. Electronic pulses were shaped at 2 μs and digitized with an analog-to-digital multichannel analyser Ortec 928-MCB.

4.4.1. Diamond-microdosimeter experimental set up and data processing

The experimental set-up was the same one adopted for the other microdosimeters. The detector sensitive volume was aligned with the centre of the ^{12}C beam and the depth in the phantom was determined by placing a stack of PMMA layers between the detector and the beam collimator. The detector has no wall, like the silicon microdosimeter.

The carbon edge in diamond is due to ions which have a range of 1 mg/cm^2; that means it is larger than the sensitive volume thickness (0.7 mg/cm^2). Therefore, the spectra were first calibrated in volts with a precision research pulser and then in keV/μm by using the carbon edge of the spectrum at 6.5 mm of PMMA depth (equivalent to 7.9 mm of water), according to the procedure described in Section 3. The lower detection threshold was ~10 keV/μm. Therefore, *f(y)* spectra have been first linearly extrapolated down to 0.01 keV/μm and then processed to obtain the yd(y) against ln(y) distributions and the $\bar{y}_D$ values.

5. The carbon ion beam line

Fig. 5 shows the 0° beam line of the Southern National Laboratories (LNS) of INFN, normally used for radiobiological experiments with carbon ions.

The irradiations were performed with a 62 MeV/u ^{12}C beam. Downstream of the vacuum window, the mono-energetic beam was spread out with two ripple filters made of PMMA (they are visible in the right side of Fig. 5 as two white standing squares), used to increase the energy spread of the mono-energetic beam and, therefore, to obtain a broader Bragg peak. The detectors were placed on the PMMA holder that is equipped with two micro-screws for an accurate alignment (left side of Fig. 5). Inside the holder, calibrated layers of PMMA (the same as those used for radiobiological measurements) were inserted to measure at different depths.

6. Dose and dose-mean let calculations

The Monte Carlo code GEANT4 version 4.9.6.p02 was used together with the advanced example “Hadrontherapy” publicly released with the GEANT4 toolkit [12] to calculate the relative absorbed dose and $L\bar{E}T_D$

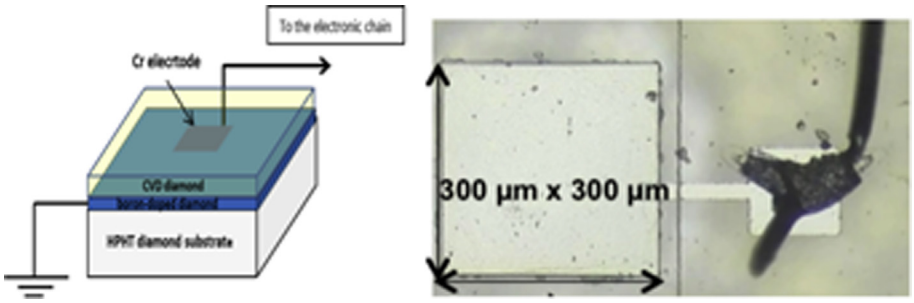

Fig. 4. Left side: schematic representation of the diamond-based microdosimeter. Right side: picture of the sensitive volume with the electrical contact towards the electronic chain.

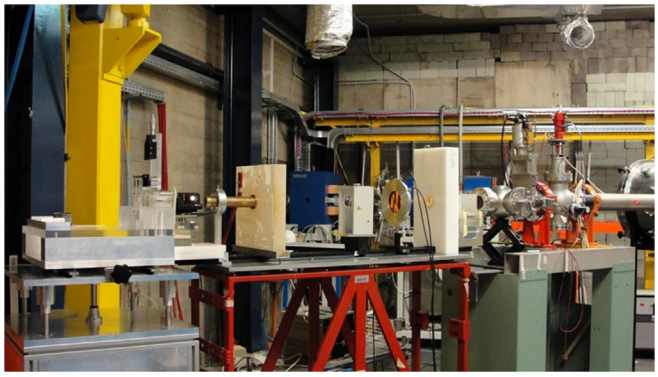

Fig. 5. The beam line at LNS that has been used for this study. The ^{12}C beam is extracted in air (right side of the figure), then it crosses the ripple filters, the first collimator, the beam monitor, the second collimator and eventually impinges on the microdosimeters, which are positioned in the PMMA detector holder on the left side of the figure.

at different depths in a water phantom, which is the reference material for dosimetry in radiation therapy. The geometry of the beam line was completely reproduced in the simulations. Primary carbon ions and all the secondary charged particles produced in elastic and inelastic collisions (i.e., all ions from oxygen to hydrogen) were transported inside the water phantom. A specific module of the application has been used to calculate $L\bar{E}T_D$ at a given water depth, weighting the dose-mean LET value of each particle with its relative dose contribution. The algorithm used is the following:

$$\bar{L}_d(z) = \frac{\sum_{j=1}^{n} \int_0^{\infty} S_{el}^{j^2}(E)\varphi_E^j(z)dE}{\sum_{j=1}^{n} \int_0^{\infty} S_{el}^{j}(E)\varphi_E^j(z)dE} \quad (4)$$

where $\bar{L}_d(z)$ is the $L\bar{E}T_D$ at the depth z in the water phantom, S_{el}^j is the electronic stopping power of the particle j of energy E and $\varphi_E^j(z)$ is the number of particles of type j that have energy E at depth z. The integral is performed over the entire energy range of the particle j and the sum is done over all charged particles set in motion by the carbon ions. More details about Monte Carlo model and its algorithms are given in reference [6].

The relative dose and $L\bar{E}T_D$ are plotted against the water depth in Fig. 6. The small circles superimposed on the relative dose curve represent the water-equivalent positions of the microdosimetric measurements. The big circle at 7.9 mm in depth shows the only common position for the four microdosimeters. The ripple filters placed in the beam line give rise to a broader Bragg peak having a FWHM of a few millimetres, with the maximum dose value occurring at a depth of 6.3 mm and a decreasing trend down to about 7.5 mm. The absorbed dose decreases then more sharply, giving rise to a "distal edge" that drops down to less than 1% of the maximum at 8.8 mm. Lighter secondary ions travel deeper into the water, giving rise to a residual and almost constant dose (~0.7% of the maximum) at higher depths.

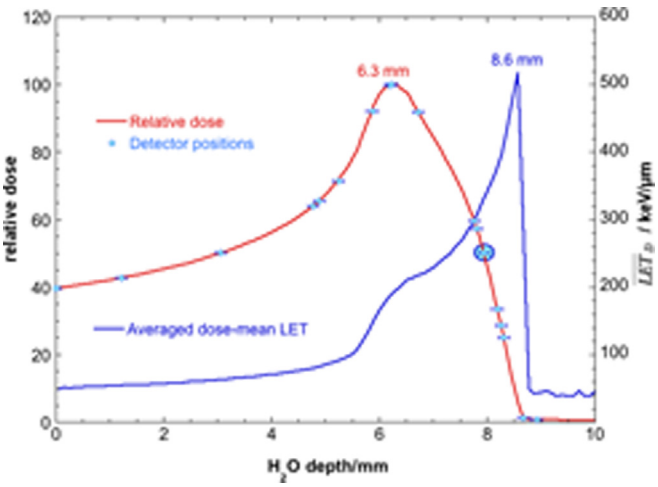

Fig. 6. Red line: relative dose as a function of the water depth. Blue line: $L\bar{E}T_D$ against water depth. Small blue circles: measurement positions, with ± 0.1 mm uncertainty. Big blue circle: measurement position common to the four detectors, where the spectra calibration has been performed. The depth values of the two curve maxima are reported. (For interpretation of the references to colour in this figure legend, the reader is referred to the web version of this article.)

The $L\bar{E}T_D$ curve shows a quasi-constant trend up to 5 mm in depth. Then, it increases sharply at the depth where also the dose increases to shape the "proximal edge" (between 5.5 and 6.5 mm). A lower LET increase is visible between about 6.5 and 7 mm in correspondence to the enlarged Bragg peak. This region is indeed characterized by a mixture of ions with different LET values, due to the effect of the ripple filters.

$L\bar{E}T_D$ increases then sharply in the region called "distal edge", up to 516 keV/µm at 8.6 mm of depth. At higher depths, the averaged dose-mean LET, which is due to the secondary charged fragments only, is almost constant, with a value of about 40 keV/µm

7. Experimental results and discussion

7.1. Microdosimetric spectra

Twenty-six measurements were performed with the four detectors, which were placed at 20 different PMMA depths. Each PMMA depth was scaled to liquid water by multiplying its value by 1.22, namely by the PMMA density (1.17 g·cm^3) and the average ratio of mass stopping power in PMMA and in water $(S/\rho)_{PMMA}/(S/\rho)_{water} = 1.047$.

The four microdosimetric spectra at 7.9 mm water-equivalent depth (calculated at the centre of the respective sensitive volumes) are shown in Fig. 7. A significant difference in the shape of the spectra can be observed. This is likely due to different particle path length distributions, caused by the different sensitive-volume shapes exposed to an approximately unidirectional radiation field, as well as by the different properties of the materials constituting the four microdosimeters.

The mini-TEPC and the GEM microdosimeter have cylindrical sensitive volumes with equal height and diameter. Their spectra are rather similar, but their different orientation with respect to the ion beam direction (the mini-TEPC axis was perpendicular to the beam, while the

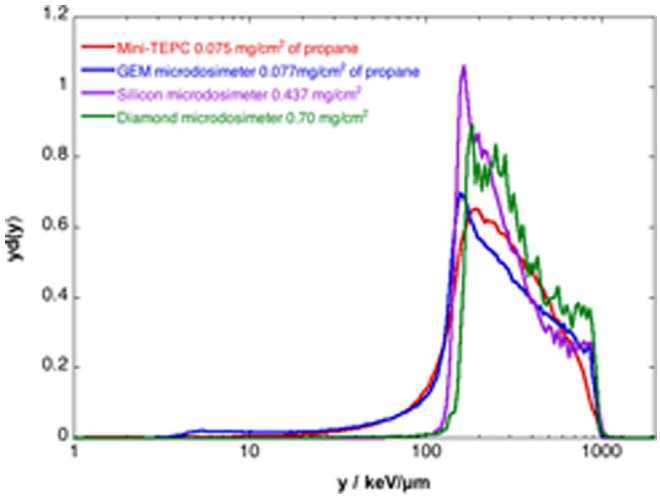

Fig. 7. Microdosimetric spectra at 7.9 mm of water-equivalent depth. In the inset legend, the sensitive volume materials of the four detectors and their mass thickness is shown.

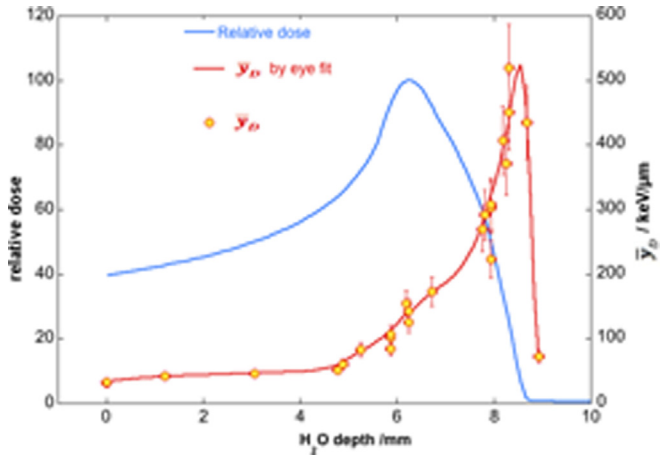

Fig. 8. Relative dose and $\bar{y}_D$ values against the depth in the water phantom. Depth uncertainty of the data is 0.1 mm and $\bar{y}_D$ uncertainty is 13%. The red line is a curve to guide the eye across the experimental data.

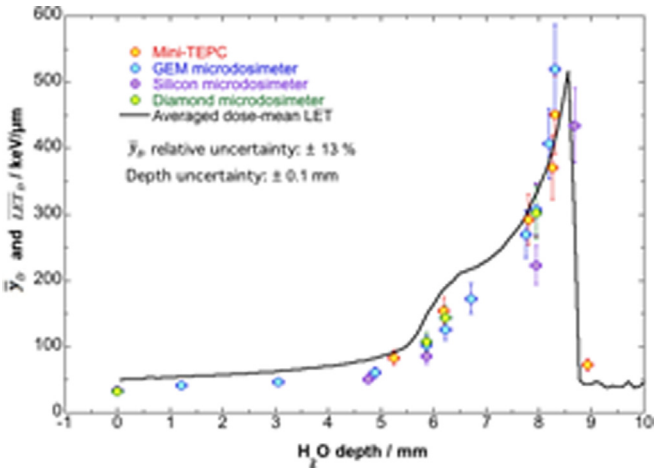

Fig. 9. $\bar{y}_D$ values and $L\bar{E}T_D$ values against the depth in the water-equivalent phantom. Circles of different colours represent $\bar{y}_D$ values of different microdosimeters. $\bar{y}_D$ uncertainty is 13%.

GEM microdosimeter axis was parallel to the beam) gives rise to a steeper carbon edge in the GEM microdosimeter. Conversely, a larger percentage of intermediate *y*-value events is present in the mini-TEPC spectrum. This is likely due to a relatively higher number of short tracks when the beam is perpendicular to the cylinder axis. Both the silicon and the diamond microdosimeters are wafers with the surface perpendicular to the beam axis. Therefore, their spectra look rather similar and their carbon edge is as steep as that of the GEM microdosimeter. With respect to gas microdosimeters, the low *y*-value component of the solid-state detector spectra is almost negligible. That is likely due to the lack of chord lengths smaller than the sensitive volume thickness. Spectra can be misshaped also by the variation of the W-value (the mean energy to create an ion pair) with the ion energy. The W-values of silicon and diamond can be assumed to be almost constant with the ion type and energy, since they have no excitation and vibration levels, but only phonons that involve only a small amount of energy. The case of propane is different, since the W-value at the carbon edge (4 MeV carbon ions) is 31.6 eV [23]. The spectra calibration procedure has implicitly used this W-value to convert the ionisation events to imparted energy, although the W-value changes with the ion type and energy. For instance, the W-value of 62 MeV/u ^{12}C ions is 27.4 eV [23]. Because of that, the same imparted energy of different ions can give rise to ionisation events of different size. Moreover, the spectra are more or less deformed with respect to the spectrum of a hypothetical liquid water microdosimeter, since the ratio $S(E)_{water}/S(E)_{material}$ varies with the ion type and energy.

A spectral correction cannot be performed, since the microdosimetric spectrum is a convolution of ionisation events due to different particles of different energies crossing different materials with different path lengths and different W-values. However, $\bar{y}_D$ can be corrected.

7.2. Dose-mean lineal energy correction

The $\bar{y}_D$ values of the spectra shown in Fig. 7 can be approximately corrected for the sensitive volume material. In fact, the measured mean imparted-energy can be scaled to water by averaging the carbon ion $S(E)_{water}/S(E)_{material}$ ratio over the entire energy range and dividing it by the same ratio calculated for the ion energy corresponding to LET_{max} in the material (carbon edge). The mean ratios were calculated by using SRIM tables [20]. The $\bar{y}_D$ correction-factors are 0.71 for silicon, 0.81 for diamond and 1.14 for propane.

The correction for the W-value variation with ion energy in propane gas can be approximately performed by averaging the W-value over the entire carbon ion energy range ($\bar{W}$ = 27.9 eV, according to Ref. [23]) and dividing it by the W-value at carbon edge (31.6 eV). Therefore, the final correction factor for $\bar{y}_D$ in propane becomes 1.007.

No correction factors have been used for the different chord length distributions.

After applying the corrections to the mean values of the spectra in Fig. 7, the four $\bar{y}_D$ values are 307, 308, 223, and 302 keV/µm for the mini-TEPC, the GEM microdosimeter, the silicon microdosimeter and the diamond microdosimeter, respectively. The average is 285 ± 41 keV/µm, where the uncertainty is the standard deviation of the data. The $\bar{y}_D$ value of the silicon microdosimeter is significantly lower than the other three values. We have not found any physical reason for this finding. However, a glance to Fig. 9, where the silicon microdosimeter data are in good agreement with all the other data, suggests that the value at 7.9 mm of depth is a simple experimental fluctuation, which needs more measurements to be reduced.

7.3. Dose-mean lineal energy uncertainties

The uncertainty on $\bar{y}_D$ values is due to several causes, the most relevant are: i) the number of spectrum counts; ii) the lower threshold value; iii) the calibration uncertainty; iv) the $\bar{y}_D$ correction factor uncertainty. Items i) and ii) give a small contribution to the total uncertainty, since all spectra have more than 10^5 counts and the relative contribution to $\bar{y}_D$ due to counts below the lower detection threshold was about 0.02% for all the detectors, except for the mini TEPC (0.2%). The calibration uncertainty is difficult to assess without an experimental study designed to analyse the accuracy of the adopted method also with carbon ions of different energy. It is similarly difficult to assess the uncertainty of item iv), since it depends on the complexity of the interaction of the mixed-radiation field with the different materials, since the ratio $S(E)_{water}/S(E)_{material}$ varies significantly with particle type and energy (e.g., in the energy range of interest, the variation is more than 40% for carbon ions impinging on silicon, while it is about 14% for propane gas). Therefore, we have taken as the overall $\bar{y}_D$ uncertainty the relative Type-A standard-uncertainty of the 13 data taken at the water-equivalent depths where measurements were carried out with more than one detector, namely at 0, 5.9, 6.2, 7.9 and 8.3 mm of depth. The $\bar{y}_D$ relative standard deviation, weighted by the number of detectors that have measured at a given depth, is 13%. This relative uncertainty has been applied to all the $\bar{y}_D$ values.

7.4. Experimental dose-mean lineal energy

The corrected $\bar{y}_D$ values with their uncertainties (13% of relative uncertainties for all the data, see Section 7.3) of all the 26

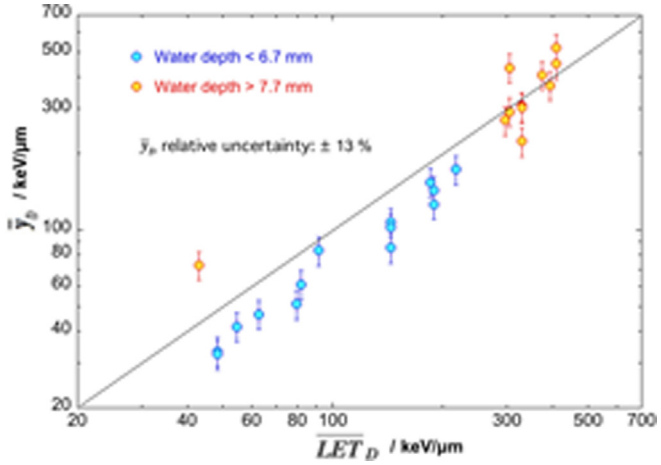

Fig. 10. $\bar{y}_D$ data of Fig. 9 plotted against $L\bar{E}T_D$ values at the same water depth. Blue symbols: measurements at water depths < 7.5 mm. Red symbols: measurements at water depths > 7.5 mm. The black line corresponds to the equality of the two variables.

measurements are plotted in Fig. 8 against the water depth. No significant differences appear in the trend of the $\bar{y}_D$ values for the four microdosimeters, in spite of the different simulated volume size (0.83 µm of water-equivalent thickness for the mini-TEPC, 0.86 µm for the GEM microdosimeter, 3.3 µm for the silicon microdosimeter and 6.1 µm for the diamond microdosimeter). This finding can be explained by the fact that all the particles cross completely the detector sensitive volumes. Therefore, the energy released inside the detectors scales, with good approximation, with their sensitive volume thicknesses.

The water depth position uncertainty was assessed to be about 0.1 mm for all the counters. A curve to guide the eye across the experimental data and the relative dose profile are also plotted in the figure. The $\bar{y}_D$ values are almost constant (41 ± 8 keV/µm) up to 4.7 mm in depth; then they show a little bump between 5 mm and 7 mm, in correspondence with the proximal edge of the spread-out Bragg peak, similarly to $L\bar{E}T_D$ (see Section 6 and Fig. 6). Then, $\bar{y}_D$ increases sharply, in correspondence of the distal edge, up to ~520 keV/µm at 8.5 mm of depth. Eventually, $\bar{y}_D$ collapses down to ~70 keV/µm at a depth of 8.9 mm.

7.5. $\bar{y}_D$-$L\bar{E}T_D$ comparison

In Fig. 9, the $\bar{y}_D$ values measured by each detector are plotted together with the calculated $L\bar{E}T_D$ values against the depth in the water phantom. As it can be clearly seen in the figure, calculated and experimental data are in rather good agreement for depths higher than 7.7 mm, namely in the absorbed-dose distal edge, where the spectra calibration has been performed. As already mentioned, no detector shows a significantly better agreement between measured $\bar{y}_D$ and calculated $L\bar{E}T_D$. On the other hand, experimental data are systematically lower than calculated ones at depths lower than 6.7 mm. No experimental measurements are available for depths between 6.7 and 7.7 mm.

The difference between the proximal and distal edge is clearer in Fig. 10, where the $\bar{y}_D$values are plotted against $L\bar{E}T_D$ calculated at the depth of measurement, together with a line showing the equality between the two variables. The average ratio between $\bar{y}_D$and $L\bar{E}T_D$ values over all the data of Fig. 10 is 0.9 ± 0.3, where the uncertainty is the standard deviation. The high relative standard-deviation (0.33) weakens the validity of equation (1). However, Fig. 10 points out that the data dispersion is greater in the distal edge region (red dots), where $\bar{y}_D = (1.1 \pm 0.3)\hat{A}\cdot L\bar{E}T_D$, while in the proximal edge and in Bragg peak region $\bar{y}_D = (0.73 \pm 0.08)\cdot L\bar{E}T_D$. Therefore, it is worthwhile to underline that all the detectors measured the same $\bar{y}_D$value up to the distal edge, since the relative data dispersion (11%) is smaller than the $\bar{y}_D$ uncertainty (13%). The larger data dispersion in the distal edge could be simply due to an insufficient accuracy of detector positioning in a region where the $\bar{y}_D$ variation in a depth of 0.1 mm is about 50 keV/µm.

The systematically lower $\bar{y}_D$-values with respect to $L\bar{E}T_D$ for depths < 6.7 mm could suggest a δ-ray escape from the detector sensitive volumes at high carbon ion energies. However, the percentage of δ-rays having a range longer than 1 µm in propane is much less than 1‰ for 62 MeV/u ^{12}C ions [24]. This is true also for silicon and diamond. On the other hand, the calibration factor that has been determined in the distal edge could be inaccurate for lower depths, due to changes in the chord length distributions. This fact can be reasonably argued, since at the distal edge the radiation field is populated by straggled carbon ions and secondary ions. However, more measurements are necessary to confirm this hypothesis. All the detectors should be placed in the same position with an accuracy better than 0.1 mm. Moreover, the measurements should be performed with larger SOBPs and higher carbon ion energies.

In these first measurements, the constructive differences of the four microdosimeters do not change the measured $\bar{y}_D$ values, within the $\bar{y}_D$ uncertainty. In order to identify the best LET monitor, new measurements with lower $\bar{y}_D$ uncertainty have to be performed.

Data show that, in these first measurements, the LET monitoring uncertainty is higher (33%) than the $\bar{y}_D$ uncertainty. This uncertainty seems to be mainly due to a change of the *k* constant (see equation (1)) in the distal edge.

8. Conclusions

The 62 MeV/u carbon ion beam of the INFN National Laboratory of Catania has been used to measure the $\bar{y}_D$ values at different depths in a PMMA phantom with four different miniaturized microdosimeters. These values have been compared to $L\bar{E}T_D$ data calculated for the same beam in a water phantom with a Monte Carlo setup based on the GEANT4 toolkit. Twenty-six measurements were performed at 20 different depths. The comparison points out a good capability of all four miniaturized microdosimeters to monitor the LET of the mixed-radiation field produced by a therapeutic carbon ion beam up to the distal edge, being the average precision 11%. However, the monitoring accuracy worsens to 33% when the distal edge data are included. Part of the data dispersion could be reduced with more precise and accurate measurements. However, a part of the data dispersion could be due to change of the proportionality factor between $\bar{y}_D$ and $L\bar{E}T_D$ at the distal edge. This hypothesis will be further studied by using higher carbon ion energies and therapeutic beams with broader spread-out Bragg peaks.

Acknowledgements

This research has been supported by the INFN within the experiment MITRA of the 5th Scientific Commission.

References

[1] PTCOG. Hadrontherapy facilities worldwide in operation, http:// www.ptcog.ch; 2017 (updated in January 2017).
[2] Raju MR, Amols HI, Bain E, Carpenter SG, Cox RA, Robertson JB. A heavy particle comparative study. Part III. OER and RBE. Br J Radiol 1978;51:712–9.
[3] Curtis SB. The OER of mixed high- and low-LET radiation. Radiat Res 1976;65:566–72.
[4] Singers Sørensen B. Overgaard J and Bassler N In vitro RBE-LET dependence for multiple particle types. Acta Oncol 2011;50:757–62.
[5] Gunzert-Marx K, Iwase H, Schardt D, Simon RS. Secondary beam fragments produced by 200 MeV u^{-1} ^{12}C ionsing water and their dose contributions in carbon ion therapy. New J Phys 2008;10:075003.
[6] Romano F, Cirrone GAP, Cuttone G, Di Rosa F, Mazzaglia SE, Petrović I, et al. A Monte Carlo study for the calculation of the average linear energy transfer (LET) distributions for a clinical proton beam line and a radiobiological carbon ion beam line. Phys Med Biol 2014;59:2863–82.
[7] ICRU. Microdosimetry. ICRU 1983; report 36.

[8] De Nardo L, Cesari V, Donà G, Magrin G, Colautti P, Conte VG, et al. Mini-TEPCs for radiation therapy. Radiat Prot Dosim 2004;108:345–52.
[9] De Nardo L, Dal Corso F, Pegoraro M. Microdosimetric measurements in gamma and neutron fields with a tissue-equivalent proportional-counter based on a gas electron multiplier. Radiat Prot Dosim 2017;175:260–6.
[10] Agosteo S, Fallica PG, Fazzi A, Introini MV, Pola A, Valvoc G. A pixelated silicon telescope for solid state microdosimetry. Radiat Meas 2008;43:585–9.
[11] Verona C, Magrin G, Solevi P, Grilj V, Jakšić M, et al. Spettroscopic properties and radiation damage investigation of a diamond based Schottky diode for ion-beam therapy microdosimetry. J Applied Phys 2015;118:184503https://doi.org/10.1063/1.4935525.
[12] Romano F, Cirrone GAP, Cuttone G, Di Rosa F, Mazzaglia SE, Sabini MG, et al. Application of Monte Carlo methods to special radiotherapeutic techniques. Nuovo Cimento C 2011;34:167–73.
[13] ICRU. Fundamental quantities and units for ionizing radiations (revised). ICRU 2011; report 35.
[14] ICRU. Quantification and reporting of low-dose and other heterogeneous exposures. ICRU 2011; report 36.
[15] Kellerer AM. An algorithm for LET-analysis. Phys Med Biol 1972;17:232–40.
[16] Colautti P, Conte V, Selva A, Chiriotti S, Pola A, Bortot D, et al. Microdosimetric study at the CNAO active-scanning carbon-ion beam. Radiat Prot Dosim 2018. https://doi.org/10.1093/rpd/ncx217.
[17] Waker AJ. Experimental uncertainties in microdosimetric measurements and an examination of performance of three commercially produced proportional counters. Nucl Instr Meth 1985;A234:354–60.
[18] Cesari V, Iborra N, De Nardo L, Querini P, Conte V, Colautti P, et al. Microdosimetric measurements of the nice therapeutic proton beam. Phys Medica 2001;XVII(Suppl. 3):76–82.
[19] Conte V, Moro D, Grosswendt B, Colautti P. Lineal energy calibration of mini tissue-equivalent gas-proportional counters (TEPC). Proceedings of Multidisciplinary Applications of Nuclear Physics With Ion Beams. AIP Conference Proceedings 2013; 1530:1: 171–8.
[20] Ziegler JF, Ziegler MD, Biersack JP. SRIM The stopping and range of ions in matter. Nucl Instr Meth 2010;B268:1818–23.
[21] Verona G, Magrin P, Solevi M, Bandorf M, Marinelli M, Stock G, et al. Toward the use of single crystal diamond based detector for ion-beam therapy microdosimetry. Radiat Meas 2018;110:25–31.
[22] Ciancaglioni I, Di Venanzio C, Marinelli M, Milani E, Prestopino G, Verona C, et al. Influence of the metallic contact in extreme-ultraviolet and soft x-ray diamond based Schottky photodiodes. J Applied Phys 2011;110:054513.
[23] Bronić IK. W values in propane-based tissue-equivalent gas. Radiat Prot Dosim 1997;70:33–6.
[24] Conte V, Colautti P, Grosswendt B, Moro D, De Nardo L. Track structure of light ions: experiments and simulations. New J Phys 2012;14:093010https://doi.org/10.1088/1367-2630/14/9/093010.